Journal of Hazardous Materials Advances 22 (2026) 101149

Contents lists available at ScienceDirect

Journal of Hazardous Materials Advances

journal homepage: www.elsevier.com/locate/hazadv

High-performance orthophosphate-modified biochar for removal of Cd (II) from aqueous solutions: Mechanisms and efficiency

Yun Chen [a,1], Xueying Li [a,1], Wenfeng Wang [a], Yazhou Feng [a], Shuming Liu [a], Aaron Albert Aryee [b], Yizhen Shao [a,*], Zhiliang Yuan [a,*]

[a] College of Life Sciences, Henan Agricultural University, No.63 Agricultural Road, Zhengzhou, 450002, China
[b] College of Basic and Applied Sciences, University of Ghana, P.O. Box LG 68, Legon, Accra, Ghana

ARTICLE INFO

Keywords:
Phosphorus modification
Biochar
Heavy metals
Adsorption
Aqueous solutions treatment

ABSTRACT

The removal of cadmium (Cd) from aqueous solutions has become a global research hotspot due to its adverse effects on human health and the ecosystem. In this study, three phosphorus-enriched biochars (PBC-1, PBC-2, and PBC-3) were produced from *Tamarix chinensis* using KH_2PO_4, $K_2HPO_4{\cdot}3H_2O$, and $K_3PO_4{\cdot}3H_2O$ as phosphate precursors, respectively. Among the synthesized materials, PBC-3 exhibited the highest Cd^{2+} removal efficiency. The adsorption of Cd^{2+} onto PBC-3 was governed by chemisorption and was well described by the pseudo-second-order kinetic model ($R^2 > 0.99$ and the lowest χ^2). At ambient temperature, PBC-3 achieved a theoretical maximum adsorption capacity of 206.94 $mg{\cdot}g^{-1}$ based on the Langmuir isotherm model ($R^2 > 0.98$ and the lowest χ^2). Additionally, the phosphorus concentration in the solution at equilibrium was found to be close to zero. PBC-3 exhibited excellent adsorption performance over a relatively wide pH range (2–8). Mechanistic investigations revealed that phosphate functional groups played a dominant role in Cd immobilization, with mineral precipitation and ion exchange accounting for 52.92 % and 42.80 % of the adsorption, respectively. Correlation analysis revealed that higher H/C, O/C, and $(N+O)$/C ratios, as well as increased specific surface area, were positively associated with Cd^{2+} uptake. This study demonstrated the advantages of $K_3PO_4{\cdot}3H_2O$-modified biochar in enhancing metal-binding capacity, highlighting its potential for the efficient treatment of Cd-contaminated aqueous solutions.

1. Introduction

Cadmium (Cd) is among the most hazardous heavy metals in industrial wastewater due to its high toxicity, strong mobility, and persistence in aquatic environments (Alzahrani et al., 2022; Chen et al., 2021). Once released, Cd accumulates in biota and transfers through the food chain, posing severe risks to ecosystems and human health (Koju et al., 2018). Cadmium accumulates in animals and plants over time, thereby affecting their growth and development (Chen et al., 2019). In addition, Long-term exposure to cadmium can lead to kidney damage, bone mineral loss, and an increased risk of cancer (Järup and Åkesson, 2009). Therefore, developing efficient, cost-effective, and environmentally friendly methods for Cd removal is crucial.

At present, a range of treatment methods—including chemical precipitation, electrochemical approaches, membrane filtration, and bioremediation—have been employed to address the challenge of heavy metal-contaminated wastewater (Fu et al., 2023). Among these approaches, adsorption has been widely applied for heavy metal removal due to its operational simplicity, relatively low cost, and high treatment efficiency (Saka et al., 2024). The adsorption process has been classified as a surface technique, suggesting that the adsorbent material plays a major role in its success (Aryee et al., 2021). In this context, biochar is a carbon-rich material produced via the pyrolysis of biomass under oxygen-limited conditions (Elhamdy, 2025). Compared to other adsorbent materials, biochar has the outstanding advantage of being derived from abundant, renewable raw materials. Waste materials can be used as raw materials to produce biochar, enabling rational, high-value utilization and achieving both economic and environmental benefits (Abdelhafez and Li, 2016; Oliveira et al., 2017). Previous studies have demonstrated that biochar can immobilize heavy metals through

* Corresponding authors.
E-mail addresses: 17737598201@163.com (X. Li), 3165853728@qq.com (W. Wang), fyz0703@163.com (Y. Feng), 410938823@qq.com (S. Liu), a.niiayi@yahoo.com (A.A. Aryee), shaoyizhen@126.com (Y. Shao), yzlsci@163.com (Z. Yuan).
[1] These authors contributed equally to this work.

https://doi.org/10.1016/j.hazadv.2026.101149
Received 9 June 2025; Received in revised form 16 March 2026; Accepted 28 March 2026
Available online 29 March 2026

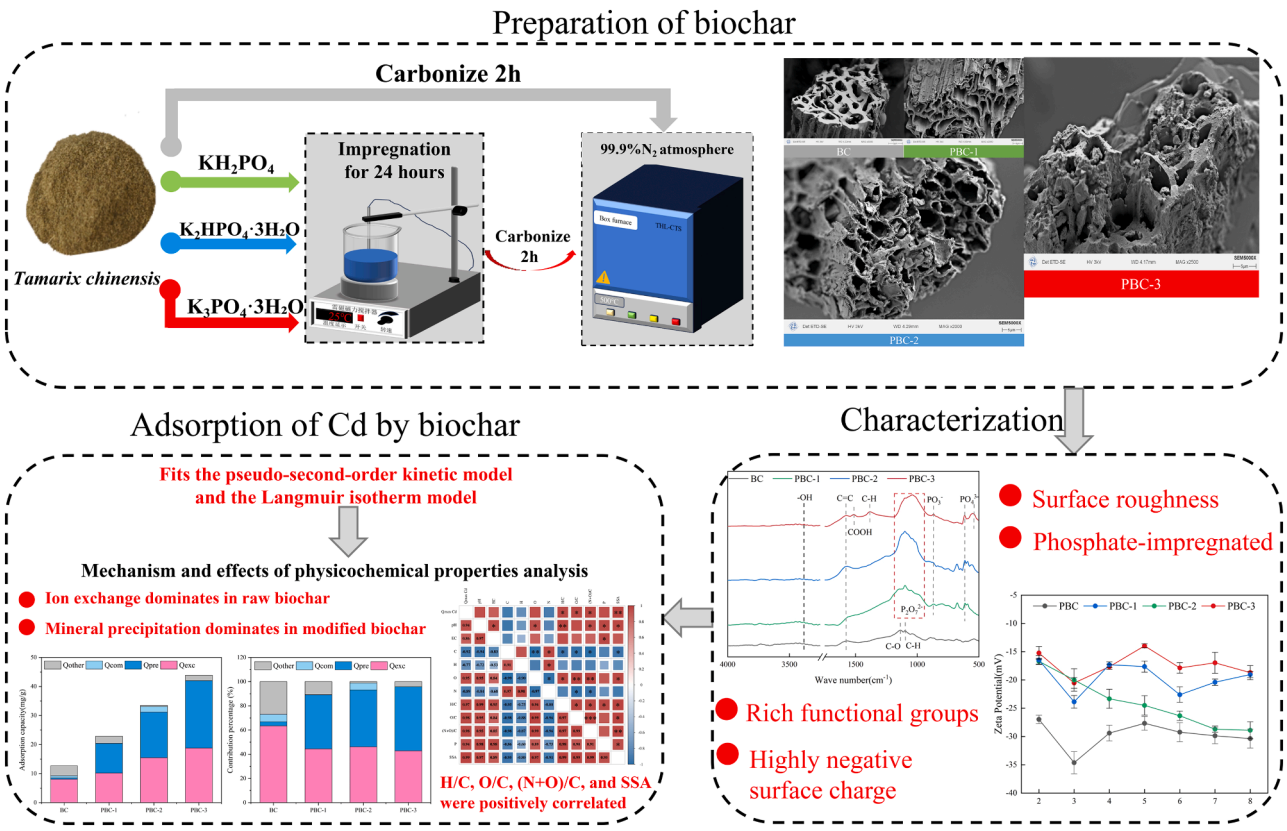

Scheme 1. Schematic diagram of the experimental workflow, including biochar preparation, physicochemical characterization, Cd (II) adsorption experiments, and mechanistic analysis.

multiple mechanisms, including cation exchange, surface complexation with oxygen-containing functional groups (Huangmee et al., 2024), and mineral precipitation (Zhang et al., 2021). In recent years, biochar derived from materials such as straw (Li et al., 2023), bamboo (Vu Thi, 2026), and sawdust (Pan et al., 2025) has been widely used to prevent and remediate Cd contamination in water. However, the practical application of raw biochar is hindered by its low adsorption capacity and environmental sensitivity (e.g., to pH and ionic strength). These limitations necessitate targeted modification strategies to enhance its Cd-binding performance.

To overcome these shortcomings, various biochar modification techniques—such as acid–base treatment (Cao et al., 2024; Shin et al., 2020), metal loading (Liu et al., 2024), and elemental doping (Dung et al., 2024)—have been extensively investigated to tailor biochar physicochemical properties (Yang et al., 2025). Among these, elemental doping using phosphorus-containing reagents has attracted considerable attention due to its high efficiency (Di et al., 2025). Phosphate-modified biochar prepared using precursors such as NaH_2PO_4 (Zhang et al., 2018), $K_3PO_4{\cdot}3H_2O$ (Wang et al., 2022), phytic acid, and sodium phytate (Di et al., 2025), shows significantly enhanced adsorption capacity for Cd^{2+} compared to raw biochar. This enhancement is generally attributed to the introduction of phosphorus functional groups, which promote Cd immobilization through surface complexation and Cd-P mineral precipitation. However, the effects of different phosphate modifications on biochar structure, phosphorus speciation, and Cd adsorption behavior have not been systematically compared. Furthermore, existing studies mostly focus on adsorption performance, while quantitative analysis of the relative contributions of various Cd removal mechanisms is often lacking. These knowledge gaps hinder a deeper understanding of the mechanisms of phosphate-enhanced cadmium adsorption and limit the rational design of high-performance biochar.

Tamarix chinensis is a woody plant widely distributed in arid or semi-arid regions of Asia, Europe, and North Africa, where it frequently proliferates in wetland and riparian ecosystems (Yan et al., 2014). Due to its strong adaptability and rapid spread, Tamarix species can outcompete native vegetation and reduce local biodiversity, and are therefore sometimes regarded as invasive or undesirable plants (Goetz et al., 2024). Owing to its soft texture and small size, Tamarix wood has limited value in conventional timber utilization. Notably, previous studies have shown that biochars derived from woody biomass generally exhibit greater structural stability and superior heavy-metal adsorption capacity than those derived from herbaceous feedstocks (Tu et al., 2022).

These characteristics suggest that Tamarix chinensis is a promising and underutilized feedstock for producing functional biochar, enabling both ecological management and value-added resource utilization. However, research on heavy metal adsorption by Tamarix-derived biochar remains scarce, and comparative studies on Tamarix-derived biochar modified with different orthophosphates are still lacking.

In this study, biochar derived from *Tamarix chinensis* was modified using three orthophosphate compounds (KH_2PO_4, $K_2HPO_4{\cdot}3H_2O$, and $K_3PO_4{\cdot}3H_2O$) to develop efficient phosphate-modified biochars for Cd^{2+} removal from aqueous solutions. The specific objectives were to: (1) characterize the physicochemical properties of pristine biochar (BC) and phosphate-modified biochars (PBC-1, PBC-2, and PBC-3); (2) compare the effects of biochars prepared with different phosphate precursors on Cd^{2+} adsorption performance and identify the optimal modification strategy; (3) the relative contributions of different Cd adsorption mechanisms were quantitatively evaluated, and the relationships between the physicochemical properties of biochar and Cd^{2+} adsorption capacity were elucidated.

2. Materials and methods

2.1. Experimental framework

In this study, biochar was synthesized from *Tamarix chinensis* biomass, including pristine biochar and biochars modified with various phosphate salts (KH_2PO_4, $K_2HPO_4{\cdot}3H_2O$, and $K_3PO_4{\cdot}3H_2O$). The resulting biochars were produced through pyrolysis and subjected to comprehensive physicochemical characterization. Their cadmium (Cd) adsorption capacities were systematically evaluated under different environmental conditions, including pH, initial Cd concentration, and contact time. In addition, the mechanisms underlying Cd adsorption by the different biochars were elucidated (Scheme 1).

2.2. Preparation and phosphorus modification of biochar

The biomass precursor for this study, tamarisk, was obtained from the Taohuayu area in the middle-to-lower reaches of the Yellow River basin. Upon collection, the plant material was thoroughly washed with deionized water, air-dried at room temperature (25 °C), ground into a fine powder, and then sieved through a 10-mesh screen. Three types of orthophosphate salts (KH_2PO_4, $K_2HPO_4{\cdot}3H_2O$, $K_3PO_4{\cdot}3H_2O$; AR, ≥99.5 %, Sinopharm Chemical Reagent Co., Ltd., China) were used to modify the tamarisk biochar. These phosphate sources all belong to the same series of potassium phosphate salts but differ in acidity and basicity, yielding different phosphorus species ($H_2PO_4^-$, HPO_4^{2-}, PO_4^{3-}) during pyrolysis. Phosphate can bind with cadmium ions to form precipitates, thereby reducing cadmium contamination (Guo et al., 2024; Wang, et al., 2025). Briefly, 10 g of ground tamarisk was mixed with 250 mL of a 0.065 mol/L solution of each orthophosphate salt for modification. The mixture was continuously stirred at ambient temperature for 24 h using a magnetic stirrer. Following this step, it was oven-dried at 60 °C and subsequently pyrolyzed in a nitrogen atmosphere (purity 99.99 %, flow rate 200 mL/min). The thermal treatment was carried out in a drawer-type furnace (THL-CTS-400×600, Henan Zhongxin Lantian Environmental Protection Equipment Co., Ltd., China), heating at a rate of 5 °C per minute until reaching 500 °C, where it was maintained for 2 h before being allowed to cool naturally to room temperature, resulting in the formation of biochar. Extensive research has shown that biochar produced at 500 °C possesses superior cadmium (Cd) adsorption capacity compared to that obtained at other pyrolysis temperatures (Yu et al., 2024). At this temperature, *Tamarix chinensis* biochar has a relatively lower ash content and higher lignocellulosic fiber content than that of other halophytic plants' biochar (Xiao et al., 2022).

The biochar prepared from raw tamarisk branches was named BC, while the biochar obtained from KH_2PO_4, $K_2HPO_4{\cdot}3H_2O$, and $K_3PO_4{\cdot}3H_2O$ modified tamarisk branches was named PBC-1, PBC-2, and PBC-3, respectively (Table S1). These samples were stored in air-tight containers and placed in a sealed desiccator before their usage.

2.3. Basic characterization of biochar properties

One gram of biochar was mixed with 25 mL of deionized water (1:2.5, w/v), and its pH and conductivity were measured using a METTLER TOLEDO FE28-Standard pH meter and a Leici DDSJ-308F conductivity meter (Li, et al., 2025; Namdari et al., 2024). The elemental contents of C, H, O, and N in the biochar samples were analyzed using an Elemental-UNICUBE elemental analyzer. The phosphorus content of biochar was determined by first digesting the sample with $HF\text{-}HNO_3\text{-}H_2O_2$, followed by spectrophotometric analysis using the molybdenum-antimony method (Zhang, et al., 2025). The surface area and pore structure of the biochar were determined using a MicrotracBEL-BELSORP MINIX surface area analyzer at 77 K for N_2 adsorption/desorption isotherms. The specific surface area of the biochar samples was determined using the Brunauer-Emmett-Teller (BET) method. At the same time, the Barrett-Joyner-Halenda (BJH) technique was employed to evaluate pore characteristics, including total pore volume, mean pore diameter, and pore size distribution. The surface morphology and elemental composition of the biochar were examined using a scanning electron microscope equipped with energy-dispersive spectroscopy (SEM-EDS, Quantum SEM 5000X + UltimMax 40). To identify the functional groups present in the biochar, both before and after Cd adsorption, Fourier transform infrared (FTIR) spectroscopy was performed using a Shimadzu IRTracer-100 instrument. X-ray diffraction (XRD) analysis on a Rigaku SmartLab SE diffractometer was used to investigate the crystalline phases and structural features of the biochar. The concentration of Cd was determined using an atomic absorption spectrometer, ZEEnit 700P (Analytik Jena AG, Germany). Additionally, the surface charge characteristics at varying pH levels were assessed by measuring zeta potential with a Malvern Zetasizer Nano ZSE.

2.4. Batch adsorption experiments

A 0.01 mol/L sodium nitrate ($NaNO_3$) solution served as the background electrolyte for preparing cadmium solutions (Wang, W.J. et al., 2025). Cadmium nitrate tetrahydrate ($Cd(NO_3)_2{\cdot}4H_2O$) was used to prepare a 50 mg/L Cd (II) solution, and its pH was carefully adjusted with 0.01 mol/L HCl or NaOH to reach the target values.

Batch adsorption tests were conducted to evaluate the Cd (II) removal performance of both raw and phosphate-modified biochars, investigating the effects of solution pH, contact time, and initial metal concentration. For pH-dependent experiments, 0.020 g of biochar was added to 20 mL of a Cd(II) solution (50 mg/L) at pH values ranging from 2 to 8. Solutions with a pH exceeding 8 were avoided, as Cd^{2+} precipitates as $Cd(OH)_2$, complicating the distinction between adsorption and precipitation (Panapitiya et al., 2025). Kinetic studies were conducted at a constant biochar dosage and initial Cd (II) concentration, with a pH of 6.0 ± 0.1 maintained and contact times ranging from 0 to 2880 min. For isotherm measurements, 0.020 g of biochar was exposed to 20 mL of Cd(II) solutions with concentrations ranging from 10 to 250 mg/L at pH 6.0 ± 0.1, and the mixtures were shaken for 24 h. Previous studies have indicated that under these conditions (solid-to-liquid ratio of 1.0 g/L, ambient temperature, and pH 6.0), Cd removal efficiency can exceed 98 % (Chen et al., 2024). After each experimental run, the suspensions were filtered using 0.45 μm nylon membranes, and the residual Cd concentration in the filtrate was quantified. The equilibrium adsorption capacity of the biochar for Cd (II), denoted as (Q_e) ($mg{\cdot}g^{-1}$), was determined according to Eq. (1):

$$Q_e = \frac{(C_0 - C_t) \times V}{m} \tag{1}$$

Q_e ($mg{\cdot}g^{-1}$) represents the equilibrium adsorption capacity of the biochar for Cd (II); C_0 ($mg{\cdot}L^{-1}$) is the initial concentration of Cd (II) in solution; C_t ($mg{\cdot}L^{-1}$) denotes the equilibrium concentration of Cd (II); V (L) refers to the total volume of the Cd (II) solution used; m (g) is the mass of biochar applied in the adsorption experiment.

2.5. Model fitting

To evaluate the kinetics of cadmium (Cd) adsorption onto the four types of biochar examined in this study, experimental data were interpreted using three kinetic models: the pseudo-first-order (Eq. (2)), pseudo-second-order (Eq. (3)), and Elovich (Eq. (4)) equations, as described by Ho and McKay et al. (Ho and McKay, 2000). The Weber-Morris intraparticle diffusion model (Eq. (5)) was used to evaluate the rate-limiting mechanism (Qu et al., 2021). For equilibrium analysis, the Langmuir (Eqs. 6), the Freundlich (Eqs. (6–7), the Temkin, and the Dubinin-Radushkevich (D-R) isotherm models were employed to characterize the adsorption behavior, as outlined in prior studies. The Temkin and D-R model fitting references the description by Damacet et al. (2026). These models were chosen to provide a comprehensive

Table 1
Basic physicochemical properties of biochar.

Sample	Yield (wt%)	pH value	EC (uS/cm)	elementary analysis (%)				atomic ratio			P ($mg{\cdot}g^{-1}$)	SSA ($m^2{\cdot}g^{-1}$)
				C	H	O	N	H/C	O/C	$(N+O)/C$		
BC	30.571	8.76	258	66.230	1.689	14.752	1.660	0.303	0.167	0.189	2.474	1.376
PBC-1	33.557	9.62	1546	70.630	1.964	13.590	2.090	0.331	0.144	0.170	20.476	2.304
PBC-2	35.653	10.71	2030	53.400	1.656	18.692	1.490	0.369	0.263	0.286	23.810	4.495
PBC-3	40.589	12.47	3060	37.640	1.434	25.188	0.800	0.453	0.502	0.520	50.252	12.076

Note: BC: raw biochar; PBC-1: KH_2PO_4-modified biochar; PBC-2: $K_2HPO_4{\cdot}3H_2O$-modified biochar; PBC-3: $K_3PO_4{\cdot}3H_2O$-modified biochar; SSA: specific Surface Area.

understanding of both kinetic and equilibrium adsorption characteristics.

$$Q_t = Q_e\left(1 - e^{-t\times K_f}\right) \tag{2}$$

$$Q_t = \frac{Q_e^2 \times K_s \times t}{1 + t \times Q_e \times K_s} \tag{3}$$

$$Q_t = K_e \ln t + C \tag{4}$$

Q_e represents the amount of Cd adsorbed by the adsorbent at adsorption equilibrium; Q_t denotes the amount of Cd adsorbed by the adsorbent at time t (min) ($mg\ g^{-1}$); K_f is the rate constant of the pseudo-first-order equation (min^{-1}); K_2 is the rate constant of the pseudo-second-order equation (g (mg min) $^{-1}$); K_e and C are the Elovich constants.

$$Qt = K_i t^{1/2} + Ci \tag{5}$$

K_i is the intraparticle diffusion rate constant ($mg\ min^{-1/2}\ g^{-1}$).

$$Q_e = \frac{Q_{max} \times K_L \times C_e}{1 + K_L \times C_e} \tag{6}$$

$$Q_e = K_F \times C_e^{1/n_F} \tag{7}$$

Q_{max} ($mg{\cdot}g^{-1}$) represents the maximum adsorption capacity of the adsorbent, while K_L ($L{\cdot}mg^{-1}$), n_F, and K_F ($mg{\cdot}g^{-1}$) are parameters related to the adsorption energy, intensity, and capacity, respectively.

2.6. Adsorption mechanism analysis

A 2 g sample of raw and phosphorus-modified biochar was placed in a conical flask containing 100 mL of 1 mol/L hydrochloric acid (Wang et al., 2015). The mixture was shaken at 200 rpm for 4 h on a constant temperature reciprocating shaker (Shanghai Boxun, BSD-TX318, benchtop intelligent precision shaker) at room temperature (25 °C) to remove most of the minerals from the biochar. This cleaning method had minimal impact on the biochar's functional groups (Cui et al., 2016). After filtration, the biochar samples were washed with distilled water until the pH stabilized and then dried at 60 °C to obtain demineralized biochar. About 0.020 g of both demineralized and raw biochar were mixed with 20 mL of a 50 mg/L Cd solution and a background solution (without Cd) at room temperature (initial pH of 6 ± 0.1), shaken for 24 h, and filtered. The concentrations of K, Na, Ca, Mg, and Cd in the filtrate were determined using an atomic absorption spectrometer (ZEEnit® 700P, Analytik, Germany). The method for quantifying the adsorption capacities of different biochars for Cd^{2+} through various mechanisms (Qcom: complexation with surface –COOH/–OH; Qexc: cation exchange; Qpre: mineral precipitation; Qother: other mechanisms) was based on the description by Wang et al. (2022). The contribution of each mechanism to Cd adsorption was determined by calculating the ratios Qpre/Qove, Qexc/Qove, Qcom/Qove, and Qoth/Qove to identify the main mechanisms of Cd adsorption across different biochars.

2.7. Data analysis

All adsorption experiments were performed in triplicate, and blank controls were conducted simultaneously to ensure the accuracy, reliability, and reproducibility of the results. Blank measurements were recorded before analysis and applied for correction when necessary. Each dataset represents the mean of three independent replicates. Standard deviations were calculated using descriptive statistics in SPSS 20.0. Adsorption kinetics and isotherm models were analyzed and plotted using Origin 2022. Heatmaps for correlation analysis were generated with R 4.3.2, whereas all other figures were prepared using Origin 2022.

3. Results and discussion

3.1. Physical and chemical properties of biochar

Compared with the raw biochar, tamarisk biochar modified with KH_2PO_4 (PBC-1), $K_2HPO_4{\cdot}3H_2O$ (PBC-2), and $K_3PO_4{\cdot}3H_2O$ (PBC-3) exhibited increased yield, pH, and electrical conductivity (EC) (Table 1). The increase in yield indicates a higher conversion efficiency of the phosphorus-modified biochar, with reduced losses of volatile substances during pyrolysis. The higher pH (Mohan et al., 2014) and electrical conductivity (EC) (Chen, H. et al., 2023) observed in the phosphate-modified biochars enhance the chemical environment, thereby providing more favorable conditions for heavy metal adsorption. In addition, compared with raw biochar (BC), PBC-1 exhibited a markedly lower H/C ratio, while PBC-2 and PBC-3 showed significantly higher O/C and $(N + O)$/C ratios, with the highest values observed in PBC-3 (Table 1). The reduction in the H/C ratio indicates enhanced surface oxidation and aromaticity in PBC-1. The elevated O/C ratios in PBC-2 and PBC-3 suggest a greater abundance of oxygen-containing functional groups on their surfaces, thereby improving hydrophilicity and enhancing adsorption capacity for water-soluble contaminants. The $(N + O)$/C ratio, a key indicator of hydrophilicity and polarity (Fonseca et al., 2025), was also significantly higher in the modified biochars, reflecting increased chemical reactivity and greater potential for applications in adsorption and environmental remediation.

Furthermore, the phosphorus levels in the modified biochars were substantially higher than those in the raw biochar. Specifically, the phosphorus concentration was measured at 2.474 mg/g in BC, while PBC-1, PBC-2, and PBC-3 exhibited significantly higher concentrations of 20.476 mg/g, 23.810 mg/g, and 50.252 mg/g, respectively. This indicates that phosphate was successfully loaded onto the biochar surface, markedly increasing its phosphorus content. This enhancement may be attributed to the presence of K^+ ions in the three phosphate salts (Zhang et al., 2018); the pore-forming effect of K^+ facilitates extensive phosphorus loading while simultaneously increasing the specific surface area (Wang et al., 2022).

3.1.1. Surface structure and porosity

SEM observations revealed that pristine BC possessed a relatively smooth surface with macroporosity, whereas phosphate-modified biochars (PBC-1, PBC-2, and PBC-3) exhibited rougher surfaces with partially collapsed or blocked pores (Fig. 1(a)). Semi-quantitative EDS analysis confirmed a substantial increase in surface phosphorus content after modification, consistent with the bulk elemental results (Fig. S1). Notably, surface roughness and phosphorus content increased progressively from PBC-1 to PBC-3, highlighting the critical role of K^+

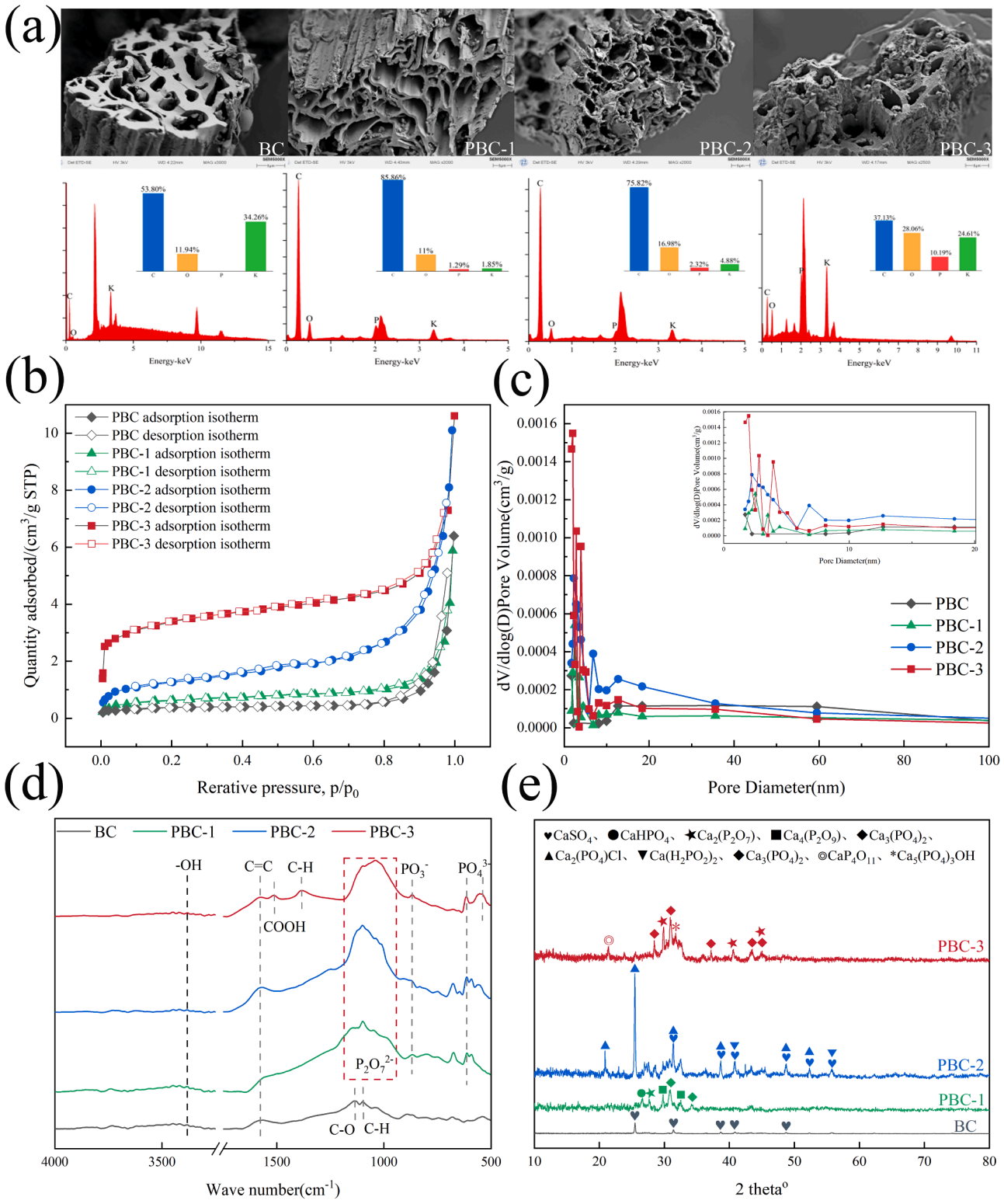

Fig. 1. Characterization of biochars: (a) SEM images with corresponding EDS elemental mapping, (b) nitrogen adsorption–desorption isotherms, (c) pore size distribution based on the BJH method, (d) FTIR spectra, and (e) XRD diffraction patterns.

concentration in promoting phosphate loading and structural reconstruction during pyrolysis.

Nitrogen adsorption–desorption analysis indicated that all biochars exhibited type III isotherms (Fig. 1(b)), suggesting weak adsorbate–adsorbent interactions and multilayer adsorption behavior (Farooq et al., 2019). The pore size distributions were dominated by mesopores (2–50 nm), with relatively few micropores (<2 nm), forming a hierarchical porous structure that is conducive to ion diffusion and surface reactions during Cd adsorption. Such hierarchical porosity facilitates efficient penetration of Cd^{2+} into internal channels and rapid access to active sites, thereby enhancing adsorption efficiency (Wang, H. et al., 2025).

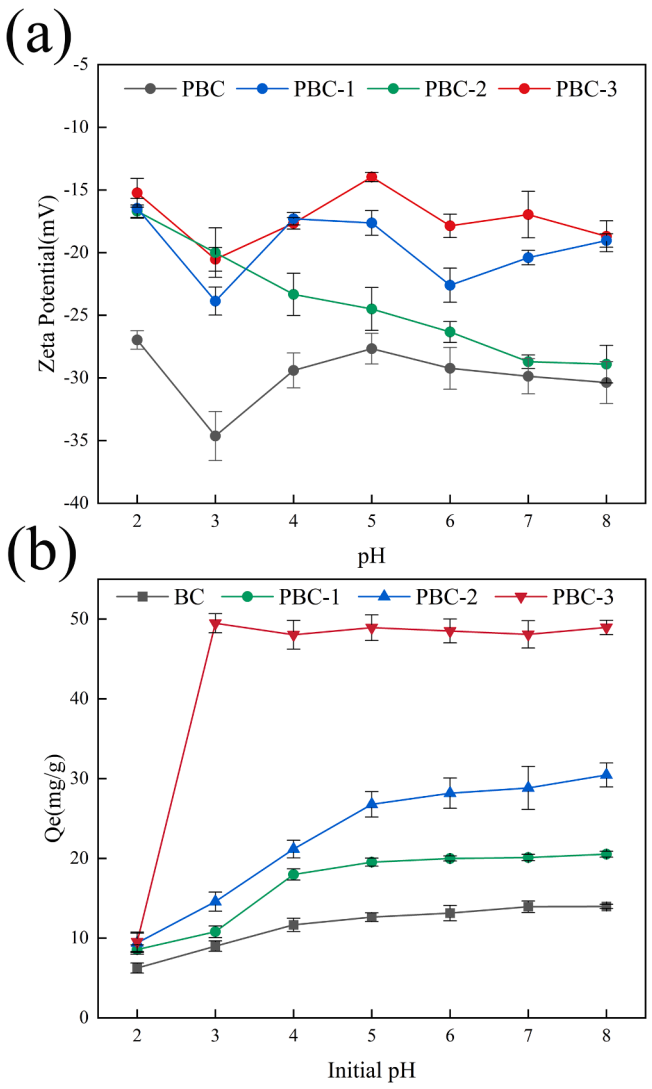

Fig. 2. Changes in Zeta potential and Cd adsorption capacity of biochars under different pH conditions.

3.1.2. *Surface chemistry and functional groups*

FTIR analysis was conducted to characterize surface functional groups of the raw and modified biochars (Fig. 1(c)). All biochars exhibited –OH absorption bands around 2800–3200 cm^{-1} (Xu et al., 2024) and aromatic *C═C* stretching vibrations around 1570 cm^{-1} (Peng et al., 2017). Compared with BC, the aromatic *C═C* peak intensity in the modified biochars was significantly enhanced, indicating a higher degree of aromatization and a more stable structure (Jin et al., 2023). PBC-3 showed a –CH peak at 1383 cm^{-1}, further indicating enhanced aromaticity, which, in turn, strengthens π–π interactions during adsorption and provides additional active sites on the biochar surface (Xu et al., 2024).

Phosphate modification introduced new acidic functional groups on the biochar surface, as evidenced by the appearance of a –COOH peak in PBC-3 around 1514 cm^{-1}. Notably, all three modified biochars exhibited strong P–O absorption peaks in the range of 1000–1200 cm^{-1}. The peaks at 551 cm^{-1} and 615 cm^{-1} correspond to PO_4^{3-} (Zhang et al., 2020), those at 1039 cm^{-1}, 1049 cm^{-1}, and 1100 cm^{-1} correspond to $P_2O_7^{4-}$, and the peak at 868 cm^{-1} corresponds to PO_3^- (Gao, R.L. et al., 2019). These results confirm the successful loading of various phosphate species, which can interact with Cd^{2+} to form Cd–P precipitates, thus enhancing adsorption.

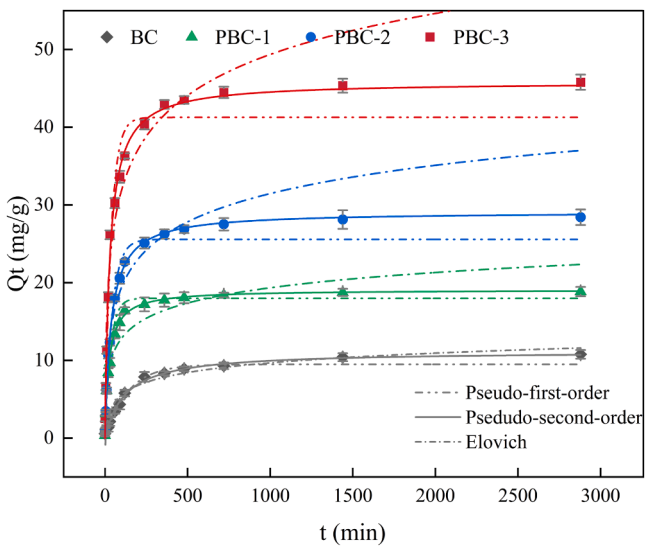

Fig. 3. Kinetic analysis of Cd adsorption behavior on biochars.

3.1.3. *Mineral composition and crystallinity*

XRD analysis was used to examine the mineral composition on the surface of the biochars (Fig. 1(e)). For BC, the 2θ diffraction peaks appeared at 25.53°, 31.42°, 38.65°, 40.87°, and 48.7°, corresponding to $CaSO_4$. For BC-1, specific diffraction peaks were well-matched with $CaHPO_4$, $Ca_2P_2O_7$, $Ca_3(PO_4)_2$, and $Ca_4P_2O_9$. For BC-2, the diffraction peaks corresponded well with $Ca_2(PO_4)Cl$, $CaSO_4$, and $Ca(H_2PO_2)_2$. For BC-3, specific diffraction peaks corresponded to CaP_4O_{11}, $Ca_3(PO_4)_2$, $Ca_2(P_2O_7)$, and $Ca_5(PO_4)_3OH$. In addition, all samples exhibit broad and weak diffraction bands in the 20–30° range, which is a typical feature of amorphous carbon.

The appearance of novel phosphorus-associated diffraction peaks in the modified biochars is likely due to the dehydration and subsequent condensation of phosphate compounds during pyrolysis at 500 °C (Padilla et al., 2023). Together with the FTIR results, these XRD patterns confirm that phosphate incorporation not only alters the surface chemistry but also introduces new crystalline domains capable of interacting with Cd^{2+}, thereby linking structural reconstruction and chemical functionality to improved adsorption performance.

3.2. *Adsorption experiments*

3.2.1. *Impact of pH and zeta potential*

Solution pH affects the chemical speciation of Cd^{2+} and the surface charge distribution of biochar (Zhang, H. et al., 2022). At pH 2.0, the adsorption capacity of Cd by all four biochars was low, possibly due to the high concentration of H^+ in the solution, which occupied surface active sites and competed with Cd^{2+} for adsorption (Kołodyńska et al., 2017). When pH ≥ 3, PBC-3 exhibited the highest adsorption capacity, which may be attributed to phosphate modification, which increased the content of acidic functional groups on the biochar surface, thereby enhancing electrostatic attraction to Cd^{2+} (Gao, R. et al., 2019).

As shown in Fig. 2(a), within the pH range of 2–8, all biochars exhibited a negative zeta potential, which is consistent with the findings of Chen et al. (2023)(Chen, Y. et al., 2023). Notably, PBC-3 exhibited the most negative zeta potential, indicating the strongest negative surface charge. Modification with orthophosphate can increase the surface content of acidic functional groups (Gao, R. et al., 2019). The strong negative charge enhances the electrostatic attraction to Cd^{2+} (Liu et al., 2025). It also increases repulsion between particles, thereby preventing aggregation and facilitating Cd^{2+} adsorption.

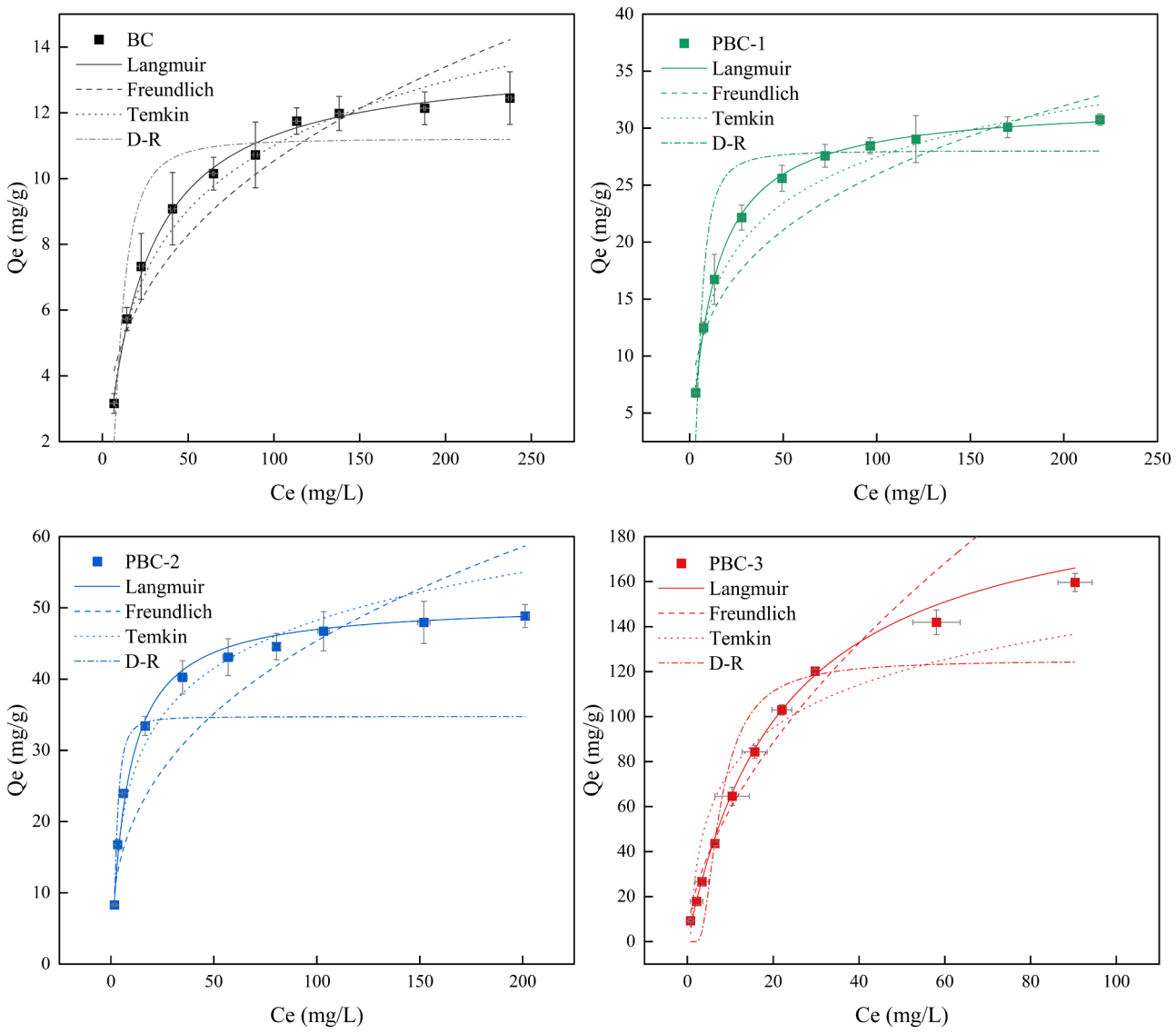

Fig. 4. Isotherm analysis of Cd adsorption behavior on biochars.

3.2.2. *Cd adsorption kinetics characteristics of biochar*

The adsorption data of raw and phosphate-modified biochars were fitted using the pseudo-first-order, pseudo-second-order, and Elovich kinetic models (Fig. 3). Compared with the pseudo-first-order model and Elovich models, the pseudo-second-order model showed a higher R^2 and a lower χ^2 (R^2= 0.990–0.998, with the lowest χ^2), indicating that Cd adsorption onto the biochars is better described by the pseudo-second-order kinetics (Table S2). The adsorption rate is predominantly governed by chemisorption. Adsorption occurred rapidly at the initial stage due to abundant active sites, followed by gradual saturation until equilibrium (Li et al., 2017). Equilibrium adsorption capacities (Qe) were 11.170 ± 0.318 mg/g for BC, 19.081 ± 0.237 mg/g for PBC-1, 29.115 ± 0.380 mg/g for PBC-2, and 45.516 ± 2.161 mg/g for PBC-3 (Table S2), clearly demonstrating the enhancement due to phosphate modification.

In addition, the Weber–Morris intraparticle diffusion model was applied to dissect further the kinetic steps involved (Fig. S2) (Azizzadeh et al., 2025). The plot exhibited multilinear behavior, which is commonly interpreted as indicative of multiple adsorption stages. The relationship between Qe and $t^{1/2}$ shows a piecewise-linear pattern and does not intersect the origin (Fig. S2 and Table S3), indicating that intraparticle diffusion is not the sole rate-limiting factor in the overall adsorption kinetics of biochar (Lu et al., 2021). Overall, the adsorption of Cd by biochar involves multiple steps, including surface adsorption, intraparticle diffusion, and potential chemisorption, each of which may be influenced by factors such as the availability of active sites, diffusion resistance, and intermolecular forces (Lu et al., 2021).

3.2.3. *Isothermal characteristics of Cd adsorption on biochar*

The adsorption isotherms of Cd^{2+} were fitted with the Langmuir and the Freundlich models (Fig. 4). The Langmuir model assumes monolayer adsorption on a homogeneous surface (Akl et al., 2022). In contrast, the Freundlich model is an empirical isotherm equation describing adsorption on heterogeneous surfaces (Masry et al., 2023). Compared with the Freundlich model, Temkin model, and D-R model, the Langmuir model exhibited a higher R^2 and a lower χ^2 (R^2= 0.988–0.999, with the lowest χ^2), indicating a better fit described by the Langmuir model (Table S4). The maximum adsorption capacities (Qmax, Langmuir) were 32.25 mg/g for PBC-1, 50.74 mg/g for PBC-2, and 206.94 mg/g for PBC-3, compared with 13.70 mg/g for BC (Table S4). Accordingly, phosphate modification increased adsorption capacity by 2.35–15.11 times, highlighting the synergistic effect of enhanced surface area, phosphate functional groups, and pore structure. Notably, PBC-3 exhibited the highest adsorption, which may be attributable to the K_3PO_4-induced

Table 2
Comparison of $Q_{e,\ cal}$ of phosphorus-modified biochars with other modified biochars for Cd^{2+}.

Modified biochars	Experimental conditions	$Q_{e,\ cal}$ (mg g^{-1})	References
Carboxyl-functionalized zirconium-based MOF	Room temperature	69.1	(Jrad et al., 2022)
Formic acid-modified zirconium-based MOF	Room temperature	34.8	(Jrad et al., 2022)
Porphyrin-based fluorescent COFs	pH = 8	166	(Jin et al., 2022)
Steel slag-biochar composites	T = 25 °C, pH = 5.0	109.21	(Wang et al., 2023)
Nano-chlorapatite wheat husks biochar	T = 25 °C, pH = 6.0	48.30	(Yuan et al., 2023)
Alkali Activation of the Cotton Straw Biochar	T = 45 °C, pH = 8.0	51.95	(Tuersun et al., 2024)
Iron-manganese modified biochar	pH = 6	75.21	(Xie et al., 2025)
Sulfhydryl-modified chitosan derivative	pH = 5.0	64.19	(Zhang, L. et al., 2025)
Magnesium-doped phosphoric acid-activated tea branch biochar	T = 25 ± 1 °C, pH = 6.0	140.43	(Lin et al., 2026)
Lactobacillus plantarum–modified biochar	T = 25 °C, pH = 6.0	12.13	(Zhu et al., 2026)
Cobalt–HHTP metal–organic framework	Room temperature	169	(Damacet et al., 2026)
PBC-3	T = 25 °C, pH = 6.0 ± 0.1	206.94	Present study

pore formation and the highest phosphorus loading, which favors the formation of Cd–P precipitates (as discussed in Section 3.3).

The equilibrium constants (K_L) ranged from 0.01 to 0.08 (Table S4), indicating favorable adsorption conditions (Worku et al., 2023). The maximum adsorption capacity of PBC-3 for Cd^{2+} in water is 1.47–17.06 times higher than that of various modified adsorbents, including MOFs and biochars (Table 2). This result further demonstrates the strong adsorption capacity of phosphorus-modified biochar for Cd.

3.3. Analysis of biochar adsorption mechanisms

Fig. 5(a) presents the FTIR spectra of different biochars after Cd adsorption. For the phosphate-modified biochars, the characteristic vibrational bands of phosphate species (e.g., PO_3^-, $P_2O_7^{4-}$, and PO_4^{3-}) showed pronounced decreases in intensity and/or noticeable peak shifts after Cd uptake. This indicates that these phosphorus-containing functional groups were directly involved in the adsorption process. During biochar pyrolysis, various oxygen- and phosphorus-containing functional groups are generated. These groups can strongly bind metal ions through surface complexation mechanisms (Zhang, P. et al., 2022). The observed FTIR variations suggest that Cd^{2+} interacts with phosphate groups on the biochar surface. This results in the formation of Cd–phosphate complexes and precipitation of cadmium phosphate phases (Guo et al., 2024).

The XRD patterns of biochars after Cd adsorption are shown in Fig. 5 (b). Diffraction peaks corresponding to $CdCO_3$ were detected, suggesting that Cd (II) can react with carbonate species or carbonate minerals present in the biochar matrix (Chen et al., 2022), a phenomenon also reported for other biochar-based adsorbents (Ye et al., 2024). After Cd^{2+} adsorption, new diffraction peaks appeared in the modified biochars. Specifically, PBC-1 exhibits good correspondence with Cd_2P_3Cl, Cd (HPO_3), Cd $(OH)_2$, and $Cd_2P_2O_7$; PBC-2 corresponds well with $CdCa_2(PO_4)_2$; and PBC-3 aligns closely with $Cd_3(PO_4)_2$. These results confirm that Cd^{2+} reacts with phosphate groups (PO_3^-, $P_2O_7^{4-}$, and PO_4^{3-}) on the modified biochars (PBC-1, PBC-2, and PBC-3).

To further elucidate the role of phosphorus in Cd removal and to evaluate the potential risk of secondary pollution, the phosphorus concentration in the equilibrium solutions of the adsorption isotherm experiments was quantified. The results showed that the phosphorus concentration in solution gradually decreased with increasing Cd adsorption, indicating that phosphorus was predominantly consumed during Cd immobilization rather than released into the aqueous phase. Previous studies have demonstrated that phosphorus-enriched biochars remove Cd mainly through phosphate complexation and precipitation mechanisms (Li et al., 2022). When the adsorption equilibrium was reached, the phosphorus concentration in all equilibrium solutions approached zero (Fig. S3), confirming that phosphate-modified biochars did not cause secondary phosphorus pollution under the experimental conditions.

The quantitative analysis of the Cd adsorption mechanisms for both raw and modified biochars is presented in Fig. 6(a) and (b). The primary mechanism of Cd adsorption by raw biochar is ion exchange, accounting for 63 % of the total adsorption capacity (8.05 mg/g). The exchangeable cations on the biochar surface, such as K^+, Ca^{2+}, Na^+, and Mg^{2+}, can undergo ion exchange with Cd^{2+} (Kukowska et al., 2025). For modified biochars, mineral precipitation is considered the dominant mechanism for Cd adsorption. The contribution of precipitation to Cd adsorption is 10.22 mg/g, 15.70 mg/g, and 23.23 mg/g, accounting for 45 %, 47 %, and 53 % of the total adsorption capacity of PBC-1, PBC-2, and PBC-3, respectively (Fig. 5(a)). This may be because the alkalinity of the modified biochar is enhanced, allowing more OH^- to combine with Cd^{2+} to form $Cd(OH)_2$ precipitates (Li and Ma, 2025). Meanwhile, the modified biochar is loaded with different phosphate ions, which combine with $Cd^{2+}$to form cadmium phosphate precipitates (Zhu et al., 2025), consistent with the previous FTIR and XRD analysis results.

Furthermore, Pearson correlation analysis showed that the H/C, O/C, $(N + O)$/C ratios, and specific surface area (SSA) of biochar were all significantly positively correlated with Cd adsorption capacity (Qmax) ($P < 0.05$). Increased O/C, H/C, and $(O + N)$/C ratios enhanced the adsorption capacity (Hafshejani and Saeidinia, 2025). Furthermore, a larger specific surface area provides more available adsorption sites (Li, R. et al., 2025), thus significantly enhancing Cd adsorption capacity. Overall, the $K_3PO_4{\cdot}3H_2O$-modified biochar (PBC-3) exhibited superior Cd(II) adsorption performance due to its enhanced physicochemical properties, including increased alkalinity, higher specific surface area, and enriched oxygen- and phosphorus-containing functional groups. These properties collectively promoted ion exchange, surface complexation, and multi-phase mineral precipitation, thereby enabling efficient immobilization and removal of Cd from aqueous solutions.

4. Conclusion

This study shows that biochars derived from Tamarix chinensis exhibit greatly improved Cd^{2+} adsorption after modification with KH_2PO_4, $K_2HPO_4{\cdot}3H_2O$, or $K_3PO_4{\cdot}3H_2O$. Among them, $K_3PO_4{\cdot}3H_2O$-modified biochar (PBC-3) performed best, with an equilibrium adsorption capacity of 206.94 mg/g, 15.11 times higher than that of the pristine biochar. Kinetic and isotherm analyses indicate that adsorption follows a pseudo-second-order kinetic model and a Langmuir isotherm, indicating chemisorption as the dominant process. Moreover, phosphorus-modified biochar maintains strong adsorption performance across a wide pH range (2–8). Mechanistic analysis indicates that while raw biochar primarily removes Cd^{2+} through ion exchange, phosphate modification enhances removal via mineral precipitation. This is achieved by forming phosphate-Cd complexes, with equilibrium phosphorus concentrations approaching zero. Correlation analysis indicated that the biochar's elemental ratios (H/C, O/C, $(N + O)$/C) and specific surface area had a significant positive influence on Cd^{2+} adsorption, explaining the superior performance of PBC-3. These results indicate that using *Tamarix chinensis* as a feedstock to produce phosphate-modified biochar is an effective method for removing Cd^{2+} from aqueous solutions. However, a limitation of this work is the lack of validation in real wastewater systems. Future research should focus on its practical performance in field applications and evaluate its

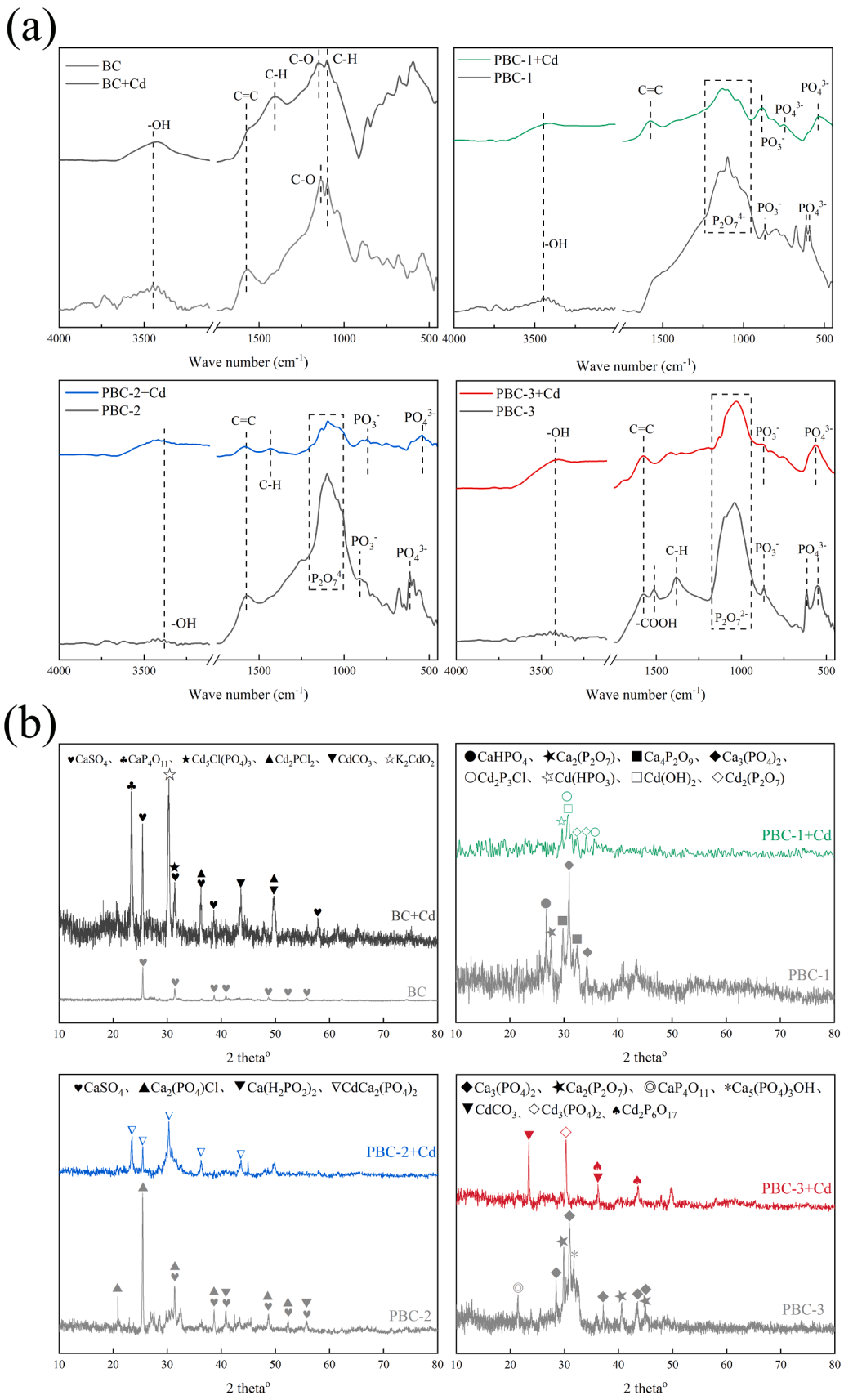

Fig. 5. (a) FTIR spectra of raw and modified biochars before and after Cd^{2+} adsorption; (b) XRD patterns of raw and modified biochars before and following Cd^{2+} adsorption.

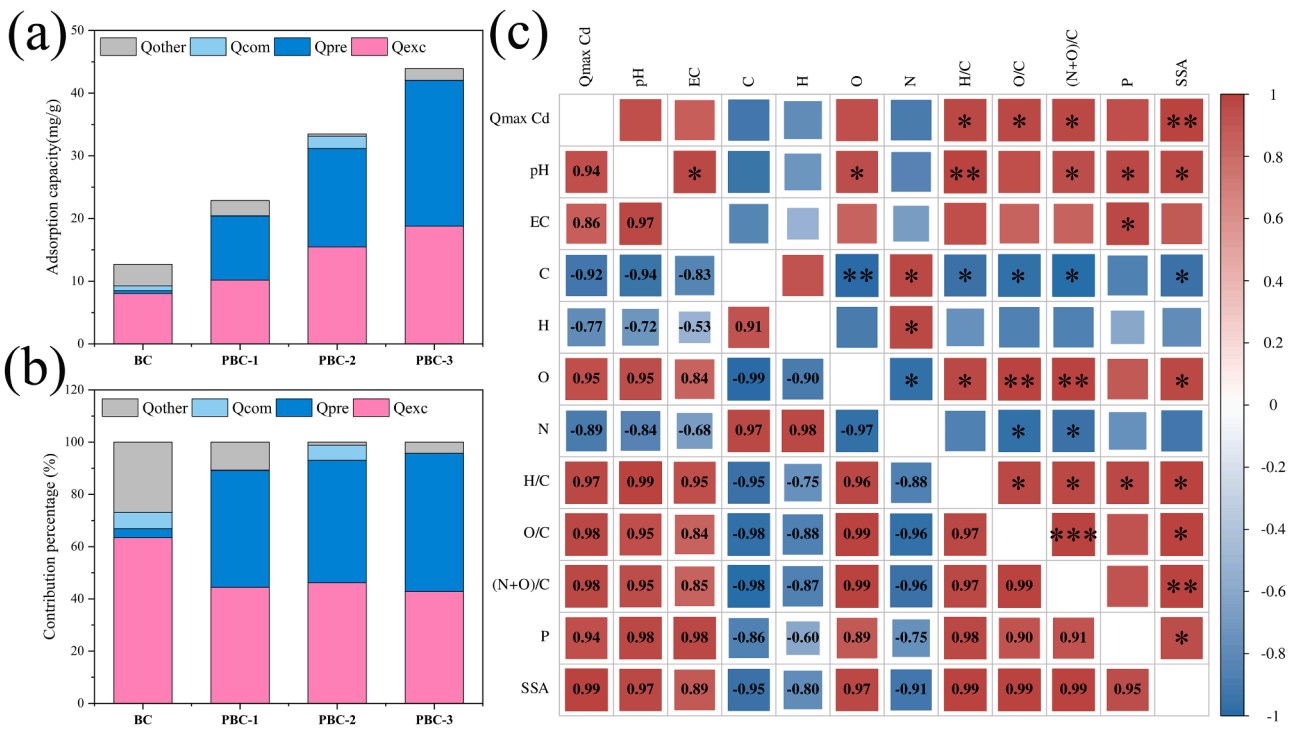

Fig. 6. (a) Cd adsorption capacities of various biochars; (b) Proportional contributions of distinct adsorption mechanisms involved in Cd removal by biochars. (c) Pearson correlation heatmap between Cd Q_{max} and the physicochemical properties of biochar. Notes: Q_{com}: Adsorption capacity attributed to complexation between Cd^{2+} and oxygen-containing functional groups (–COOH, –OH) on the biochar surface. Q_{exc}: Adsorption capacity due to cation exchange, i.e., release of K^+, Na^+, Ca^{2+}, and Mg^{2+} from biochar in exchange for Cd^{2+}. Q_{pre}: Adsorption capacity due to mineral precipitation, where Cd^{2+} is immobilized as insoluble mineral phases (e.g., phosphates or carbonates). Q_{other}: Adsorption capacity from other mechanisms not covered above, such as physical adsorption or micropore diffusion. In (c), red and blue colors indicate negative and positive correlations, respectively; the size of each square represents the strength of the correlation, * indicates $P < 0.05$, ** indicates $P < 0.01$, and *** indicates $P < 0.001$.

effectiveness in removing Cd(II) from tap water, rainwater, rivers, and other natural water bodies.

Funding information

This work was supported by the Yellow River Basin Biodiversity Survey, Observation and Assessment Project (No. 30803664); the Key Scientific Research Project Plan of Colleges and Universities in Henan Province (No. 24A180013); and the Young Backbone Teachers Training Program of Universities in Henan Province (No. 2024GGJS026).

CRediT authorship contribution statement

Yun Chen: Investigation, Formal analysis, Data curation. **Xueying Li:** Writing – original draft, Validation, Software, Investigation, Formal analysis. **Wenfeng Wang:** Methodology. **Yazhou Feng:** Formal analysis, Data curation. **Shuming Liu:** Formal analysis, Data curation. **Aaron Albert Aryee:** Writing – review & editing. **Yizhen Shao:** Supervision, Methodology, Funding acquisition. **Zhiliang Yuan:** Writing – review & editing, Supervision, Project administration, Funding acquisition.

Declaration of competing interest

The authors declare that they have no known competing financial interests or personal relationships that could have appeared to influence the work reported in this paper.

Acknowledgments

This work was supported by the Yellow River Basin Biodiversity Survey, Observation and Assessment Project (No. 30803664); the Key Scientific Research Project Plan of Colleges and Universities in Henan Province (No. 24A180013); and the Young Backbone Teachers Training Program of Universities in Henan Province (No. 2024GGJS026).

Supplementary materials

Supplementary material associated with this article can be found, in the online version, at doi:10.1016/j.hazadv.2026.101149.

Data availability

Data will be made available on request.

References

Abdelhafez, A.A., Li, J., 2016. Removal of Pb(II) from aqueous solution by using biochars derived from sugar cane bagasse and orange peel. J. Taiwan Inst. Chem. Eng. 61, 367–375. https://doi.org/10.1016/j.jtice.2016.01.005.

Akl, M.A., Hashem, M.A., Ismail, M.A., Abdelgalil, D.A., 2022. Novel diaminoguanidine functionalized cellulose: synthesis, characterization, adsorption characteristics and application for ICP-AES determination of copper(II), mercury(II), lead(II) and cadmium(II) from aqueous solutions. Bmc Chem. 16 (1). https://doi.org/10.1186/s13065-022-00857-3.

Alzahrani, O.M., Abo-Amer, A.E., Mohamed, R.M., 2022. Improvement of Zn (II) and Cd (II) biosorption by Priestia megaterium PRJNA526404 isolated from agricultural waste water. Microorganisms. 10 (12). https://doi.org/10.3390/microorganisms10122510.

Aryee, A.A., Dovi, E., Han, R.P., Li, Z.H., Qu, L.B., 2021. One novel composite based on functionalized magnetic peanut husk as adsorbent for efficient sequestration of phosphate and Congo red from solution: characterization, equilibrium, kinetic and mechanism studies. J. Colloid. Interface Sci. 598, 69–82. https://doi.org/10.1016/j.jcis.2021.03.157.

Azizzadeh, S.E., Bariki, S.G., Movahedirad, S., 2025. Magnetic orange leaf biochar for favipiravir removal from wastewater. Sci. Rep. 15 (1). https://doi.org/10.1038/s41598-025-11631-5.

Cao, B., Li, M., Zhang, T., Gong, T., Yang, T., Xi, B., Lu, H., Wang, Z., 2024. Dynamics and mechanisms of atrazine adsorption on biogas-residue biochar with citric acid modification. Sep. Purif. Technol. 337, 126151. https://doi.org/10.1016/j.seppur.2023.126151.

Chen, H., Li, Y., Ma, X., Guo, L., He, Y., Ren, Z., Kuang, Z., Zhang, X., Zhang, Z., 2019. Analysis of potential strategies for cadmium stress tolerance revealed by transcriptome analysis of upland cotton. Sci. Rep. 9 (1), 86. https://doi.org/10.1038/s41598-018-36228-z.

Chen, H., Min, F., Hu, X., Ma, D., Huo, Z., 2023a. Biochar assists phosphate solubilizing bacteria to resist combined Pb and Cd stress by promoting acid secretion and extracellular electron transfer. J. Hazard. Mater 452, 131176. https://doi.org/10.1016/j.jhazmat.2023.131176.

Chen, K., Ma, D., Yu, H., Zhang, S., Seyler, B.C., Chai, Z., Peng, S., 2022. Biosorption of V (V) onto Lantana camara biochar modified by H3PO4: characteristics, mechanism, and regenerative capacity. Chemosphere 291, 132721. https://doi.org/10.1016/j.chemosphere.2021.132721.

Chen, M.L., Liu, H.Y., Pan, J.Q., He, S.M., Hong, Y., Wang, S.W., Zhou, Y., Chen, D.Y., Su, M.H., 2024. Enhanced cadmium removal by a magnetic potassium ferrocyanide framework: performance and mechanism study. Ecotoxicol. Env. Saf 282. https://doi.org/10.1016/j.ecoenv.2024.116702.

Chen, R.H., Zhang, Q.R., Chen, H.Y., Yue, W.F., Teng, Y.G., 2021. Source apportionment of heavy metals in sediments and soils in an interconnected river-soil system based on a composite fingerprint screening approach. J. Hazard. Mater 411. https://doi.org/10.1016/j.jhazmat.2021.125125.

Chen, Y., Mao, W., Yang, W., Niazi, N.K., Wang, B., Wu, P., 2023b. A novel phosphate rock-magnetic biochar for Pb2+ and Cd2+ removal in wastewater: characterization, performance and mechanisms. Environ. Technol. Innov. 32, 103268. https://doi.org/10.1016/j.eti.2023.103268.

Cui, X.Q., Fang, S.Y., Yao, Y.Q., Li, T.Q., Ni, Q.J., Yang, X.E., He, Z.L., 2016. Potential mechanisms of cadmium removal from aqueous solution by *Canna indica*derived biochar. Sci. Total Environ. 562, 517–525. https://doi.org/10.1016/j.scitotenv.2016.03.248.

Damacet, P., Shehayeb, E.O., Monti, S., Barcaro, G., Mirica, K.A., 2026. Redox-active metal–Organic framework nanocrystals for the simultaneous adsorption, detection, and detoxification of heavy metal cations. ACS. Appl. Mater. Interfaces. 18 (1), 1218–1230. https://doi.org/10.1021/acsami.5c18562.

Di, D., Xiao, J., Zhao, B., Chen, Y., Song, Z., Chen, G., 2025. Immobilization of Cd(II) by phosphorus-modified bamboo biochar from solution: mechanistic study from qualitative to quantitative analysis. Carbon Res. 4 (1), 35. https://doi.org/10.1007/s44246-025-00196-7.

Dung, N.T., Thao, V.D., Thao, N.P., Thuy, C.T.M., Nam, N.H., Ngan, L., Lin, K.Y.A., Khiem, T.C., Huy, N.N., 2024. Turning peroxymonosulfate activation into singlet oxygen-dominated pathway for ofloxacin degradation by co-doping N and S into durian peel-derived biochar. Chem. Eng. J. 483. https://doi.org/10.1016/j.cej.2024.149099.

Elhamdy, W.A., 2025. Environmental sustainable ZrO2 -phosphorous biochar nano composite derived from sugarcane bagasse and their adsorption behavior of antidepressant drugs. BMC Chem. 19 (1), 68. https://doi.org/10.1186/s13065-025-01430-4.

Farooq, U., Phul, R., Alshehri, S.M., Ahmed, J., Ahmad, T., 2019. Electrocatalytic and enhanced photocatalytic applications of Sodium niobate nanoparticles developed by Citrate precursor route. Sci. Rep. 9. https://doi.org/10.1038/s41598-019-40745-w.

Fonseca, J.D.D., Matej-Lukowicz, K., Kluska, J., Baluk, M.A., Kulesza, J., Barros, B.S., Wojciechowska, E., 2025. Effect of synthesis method on ammonium sorption behavior of oat husk biochar. Sci. Rep. 15 (1). https://doi.org/10.1038/s41598-025-89335-z.

Fu, P., Wang, X., Shi, J., Zhou, L.X., Hou, Q.J., Wang, W.Q., Tian, Y., Qin, J.M., Bi, W.L., Liu, F.W., 2023. Enhanced removal of As(III) and Cd(II) from wastewater by alkali-modified Schwertmannite@Biochar. Environ. Technol. Innov. 31. https://doi.org/10.1016/j.eti.2023.103197.

Gao, R., Fu, Q., Hu, H., Wang, Q., Liu, Y., Zhu, J., 2019a. Highly-effective removal of Pb by co-pyrolysis biochar derived from rape straw and orthophosphate. J. Hazard. Mater 371, 191–197. https://doi.org/10.1016/j.jhazmat.2019.02.079.

Gao, R.L., Fu, Q.L., Hu, H.Q., Wang, Q., Liu, Y.H., Zhu, J., 2019b. Highly-effective removal of Pb by co-pyrolysis biochar derived from rape straw and orthophosphate. J. Hazard. Mater 371, 191–197. https://doi.org/10.1016/j.jhazmat.2019.02.079.

Goetz, A.R.B., González-Sargas, E., Vidal, M.C., Shafroth, P.B., Henry, A.L., Sher, A.A., 2024. Outcomes of control and monitoring of a widespread riparian invader (Tamarix spp.): a comparison of synthesis approaches. NeoBiota 91, 67–98. https://doi.org/10.3897/neobiota.91.111628.

Guo, K.X., Zhao, Y.H., Zhang, Y., Yang, J.B., Chu, Z.Y., Zhang, Q., Xiao, W.W., Huang, B., Li, T.Y., 2024. Effects of wollastonite and phosphate treatments on cadmium bioaccessibility in pak choi (Brassica rapa L. ssp. chinensis) grown in contaminated soils. Front. Nutr. 11. https://doi.org/10.3389/fnut.2024.1337996.

Hafshejani, L.D., Saeidinia, M., 2025. Integrating chemical modification pathways and machine learning for optimization of nitrate removal by rapeseed (Brassica napus L.) biochar. Sci. Rep. 16 (1), 447. https://doi.org/10.1038/s41598-025-29743-3.

Ho, Y.S., McKay, G., 2000. The kinetics of sorption of divalent metal ions onto sphagnum moss peat. Water. Res. 34 (3), 735–742. https://doi.org/10.1016/S0043-1354(99)00232-8.

Huangmee, K., Hsu, L.-C., Tzou, Y.-M., Cho, Y.-L., Liao, C.-H., Teah, H.Y., Liu, Y.-T., 2024. Thiol-functionalized black carbon as effective and economical materials for Cr (VI) removal: simultaneous sorption and reduction. J. Env. Manage 360, 121074. https://doi.org/10.1016/j.jenvman.2024.121074.

Järup, L., Åkesson, A., 2009. Current status of cadmium as an environmental health problem. Toxicol. Appl. Pharmacol 238 (3), 201–208. https://doi.org/10.1016/j.taap.2009.04.020.

Jin, R.T., Zhao, C.L., Song, Y.X., Qiu, X.J., Li, C.X., Zhao, Y.X., 2023. Competitive adsorption of sulfamethoxazole and bisphenol A on magnetic biochar: mechanism and site energy distribution. Env. Pollut 329, 10. https://doi.org/10.1016/j.envpol.2023.121662.

Jin, W.-L., Li, W., Wang, H.-X., Liu, X.-W., Jiang, H.-X., Zhu, L.-N., Kong, D.-M., 2022. Sponge-supported monolithic materials of porphyrin covalent organic frameworks for selective recognition, convenient removal and extraction of Cd2+. J. Environ. Chem. Eng. 10 (3), 107662. https://doi.org/10.1016/j.jece.2022.107662.

Jrad, A., Damacet, P., Yaghi, Z., Ahmad, M., Hmadeh, M., 2022. Zr-based metal–Organic framework nanocrystals for water remediation. ACS Appl. Nano Mater. 5 (8), 10795–10808. https://doi.org/10.1021/acsanm.2c02128.

Koju, N.K., Song, X., Wang, Q., Hu, Z.H., Colombo, C., 2018. Cadmium removal from simulated groundwater using alumina nanoparticles: behaviors and mechanisms. Env. Pollut 240, 255–266. https://doi.org/10.1016/j.envpol.2018.04.107.

Kołodyńska, D., Bąk, J., Kozioł, M., Pylychuk, L.V., 2017. Investigations of heavy metal ion sorption using nanocomposites of iron-modified biochar. Nanoscale Res. Lett. 12 (1), 433. https://doi.org/10.1186/s11671-017-2201-y.

Kukowska, S., Nowicki, P., Szewczuk-Karpisz, K., 2025. New fruit waste-derived activated carbons of high adsorption performance towards metal, metalloid, and polymer species in multicomponent systems. Sci. Rep. 15 (1). https://doi.org/10.1038/s41598-025-85409-0.

Li, H., Dong, X., da Silva, E.B., de Oliveira, L.M., Chen, Y., Ma, L.Q., 2017. Mechanisms of metal sorption by biochars: biochar characteristics and modifications. Chemosphere 178, 466–478. https://doi.org/10.1016/j.chemosphere.2017.03.072.

Li, L.F., Ma, Y.X., 2025. Rhizosphere effects on cadmium fractionation in contaminated soils: a comparative study of ultisols and alfisols. Sci. Rep. 15 (1). https://doi.org/10.1038/s41598-025-14241-3.

Li, P., Ding, S., Xin, X., Zhu, A., Ding, S., Mei, Y., Liu, Y., Wu, X., Lu, K., Zhao, Q., 2025a. Ecological niche differentiation of detritivores dominates soil mesofaunal community assembly in a 33-year fertilized cropland. Soil Tillage Res. 252, 106605. https://doi.org/10.1016/j.still.2025.106605.

Li, R., Xia, L., Yue, J., Wu, J., Teng, X., Chen, J., Huang, G., Wang, J., Pan, F., 2025b. Nanosized anatase TiO2 with exposed (001) facet for high-capacity Mg2+ ion storage in magnesium ion batteries. Nano-Micro Lett. 18 (1), 17. https://doi.org/10.1007/s40820-025-01861-7.

Li, S., Luo, C., Yan, F., Yang, Y., Guo, B., Wang, L., Xu, S., Wu, F., Ji, P., 2023. Remediation of Pb(II) and Cd(II) in polluted waters with calcium thioglycolate–modified straw biochar. Env. Pollut 338, 122638. https://doi.org/10.1016/j.envpol.2023.122638.

Li, X., Huang, Y., Liang, X., Huang, L., Wei, L., Zheng, X., Albert, H.A., Huang, Q., Liu, Z., Li, Z., 2022. Characterization of biochars from woody agricultural wastes and sorption behavior comparison of cadmium and atrazine. Biochar. 4 (1), 27. https://doi.org/10.1007/s42773-022-00132-7.

Lin, D., Xu, H., Ren, Y., Teng, T., Qian, Z., He, J., 2026. Magnesium-doped phosphoric acid-activated tea branch biochar for efficient removal of Cd2+ and Pb2+ from water: adsorption behavior and insight into the quantitative mechanism. Langmuir. 42 (9), 6835–6847. https://doi.org/10.1021/acs.langmuir.5c06111.

Liu, H., Zhang, X., Hou, R., Chen, G., Fang, Y., Zhang, J., Liu, L., Liu, L., 2025. Ultrasonic assisted preparation of covalent bonding pea protein and polyphenol conjugate in emulsion delivery system. Int. J. Biol. Macromol 287, 138442. https://doi.org/10.1016/j.ijbiomac.2024.138442.

Liu, J.H., Zhu, J.F., Zeng, X.C., Yang, Y.X., Zhang, G.H., Sun, Y.H., Fan, G.D., 2024. Enhanced activation of persulfate by bimetal and nitrogen co-doped biochar for efficient degradation of refractory organic contaminants: the role of the second metal. J. Phys. Chem. Solids 193. https://doi.org/10.1016/j.jpcs.2024.112191.

Lu, Z., Zhang, H., Shahab, A., Zhang, K., Zeng, H., Bacha, A.-U.-R., Nabi, I., Ullah, H., 2021. Comparative study on characterization and adsorption properties of phosphoric acid activated biochar and nitrogen-containing modified biochar employing Eucalyptus as a precursor. J. Clean. Prod. 303, 127046. https://doi.org/10.1016/j.jclepro.2021.127046.

Masry, B.A., Elgoud, E.M.A., Riz, S.E., 2023. Modeling and equilibrium studies on the recovery of praseodymium (III), dysprosium (III) and yttrium (III) using acidic cation exchange resin (vol 16, 37, 2022). Bmc Chem. 17 (1). https://doi.org/10.1186/s13065-023-00940-3.

Mohan, D., Sarswat, A., Ok, Y.S., Pittman, C.U., 2014. Organic and inorganic contaminants removal from water with biochar, a renewable, low cost and sustainable adsorbent – A critical review. Bioresour. Technol 160, 191–202. https://doi.org/10.1016/j.biortech.2014.01.120.

Namdari, M., Soleimani, M., Mirghaffari, N., Kharrazi, S.M., 2024. Effect of biological sewage sludge and its derived biochar on accumulation of potentially toxic elements by corn (Zea mays L.). Sci. Rep. 14 (1), 5985. https://doi.org/10.1038/s41598-024-56652-8.

Oliveira, F.R., Patel, A.K., Jaisi, D.P., Adhikari, S., Lu, H., Khanal, S.K., 2017. Environmental application of biochar: current status and perspectives. Bioresour. Technol 246, 110–122. https://doi.org/10.1016/j.biortech.2017.08.122.

Padilla, J.T., Watts, D.W., Novak, J.M., Cerven, V., Ippolito, J.A., Szogi, A.A., Johnson, M.G., 2023. Magnesium activation affects the properties and phosphate sorption capacity of poultry litter biochar. Biochar. 5 (1). https://doi.org/10.1007/s42773-023-00263-5.

Pan, X., Kuang, S.P., Wang, X., Ullah, H., Rao, Z.P., Ali, E.F., Abbas, Q., Lee, S.S., Shaheen, S.M., 2025. Functionalization of sawdust biochar using Mg-Fe-LDH and sodium dodecyl sulfonate enhanced its stability and immobilization capacity for Cd

and Pb in contaminated water and soil. Biochar. 7 (1). https://doi.org/10.1007/s42773-024-00401-7.
Panapitiya, P.H.P., Weerakoon, T., Fernando, M.S., Wimalasiri, A., de Silva, K.M.N., de Silva, R.M., 2025. Graphene oxide - polymer nanocomposites for efficient water hardness removal: a step towards healthier drinking water. RSC. Adv. 15 (33), 27356–27368. https://doi.org/10.1039/d5ra00562k.
Peng, H.B., Gao, P., Chu, G., Pan, B., Peng, J.H., Xing, B.S., 2017. Enhanced adsorption of Cu(II) and Cd(II) by phosphoric acid-modified biochars. Env. Pollut 229, 846–853. https://doi.org/10.1016/j.envpol.2017.07.004.
Qu, J.H., Wang, Y.X., Tian, X., Jiang, Z., Deng, F.X., Tao, Y., Jiang, Q., Wang, L., Zhang, Y., 2021. KOH-activated porous biochar with high specific surface area for adsorptive removal of chromium (VI) and naphthalene from water: affecting factors, mechanisms and reusability exploration. J. Hazard. Mater 401. https://doi.org/10.1016/j.jhazmat.2020.123292.
Saka, C., Tegin, I., Kahvecioglu, K., Yavuz, O., 2024. Nitrogen- and oxygen-doped carbon particles produced from almond shells by hydrothermal method for efficient Pb(II) and Cd(II) adsorption. Biomass Convers. Biorefinery 14 (15), 17467–17480. https://doi.org/10.1007/s13399-023-03920-8.
Shin, J., Lee, Y.-G., Lee, S.-H., Kim, S., Ochir, D., Park, Y., Kim, J., Chon, K., 2020. Single and competitive adsorptions of micropollutants using pristine and alkali-modified biochars from spent coffee grounds. J. Hazard. Mater 400, 123102. https://doi.org/10.1016/j.jhazmat.2020.123102.
Tu, P.F., Zhang, G.L., Wei, G.Q., Li, J., Li, Y.Q., Deng, L.F., Yuan, H.R., 2022. Influence of pyrolysis temperature on the physicochemical properties of biochars obtained from herbaceous and woody plants. Bioresour. Bioprocess. 9 (1). https://doi.org/10.1186/s40643-022-00618-z.
Tuersun, N., Wang, Y., Aihemaiti, A., Wang, J., Huang, C., 2024. Effects of Alkali activation of the cotton straw biochar on the adsorption performance for Cd2+. ACS. Omega 9 (16), 17989–18000. https://doi.org/10.1021/acsomega.3c09501.
Vu Thi, H., 2026. Mechanistically validated selective adsorption of pb(II), cd(II), and hg (II) on thiol-functionalized hierarchical magnetic biochar under competitive conditions. Sep. Purif. Technol. 388, 136860. https://doi.org/10.1016/j.seppur.2026.136860.
Wang, H., Cao, C., Chen, J., Zhou, G., Liu, T., Yuan, Y., Wang, N., 2025a. Hierarchical triple-channel architectures unlock scalable and high-efficient uranium extraction from seawater. Nat. Commun. 16 (1), 10799. https://doi.org/10.1038/s41467-025-65835-4.
Wang, J., Sun, Q., Wang, M.Y., Wang, J.H., Yang, Y.X., Wu, J.Z., Zhao, K.L., 2025b. Combined application of calcium fertilizer improves the immobilization of biochar-ferromanganese materials on cd/as co-polluted paddy soils under acidifying conditions. Sci. Rep. 15 (1). https://doi.org/10.1038/s41598-025-08663-2.
Wang, M., Wang, X., Zhang, M., Han, W., Yuan, Z., Zhong, X., Yu, L., Ji, H., 2023. Treatment of Cd(II) and As(V) co-contamination in aqueous environment by steel slag-biochar composites and its mechanism. J. Hazard. Mater 447, 130784. https://doi.org/10.1016/j.jhazmat.2023.130784.
Wang, Q., Duan, C.J., Xu, C.Y., Geng, Z.C., 2022. Efficient removal of Cd(II) by phosphate-modified biochars derived from apple tree branches: processes, mechanisms, and application. Sci. Total Environ. 819. https://doi.org/10.1016/j.scitotenv.2021.152876.
Wang, W.J., Jiang, H.Y., Tan, Z.B., Yu, L.Y., Chen, J., Xiao, Q.L., Rong, Q.L., Zhou, C.H., 2025c. Selenium-modified biochar synergistically achieves the safe use of Selenium and the inhibition of heavy metal cadmium. Molecules. 30 (2). https://doi.org/10.3390/molecules30020347.
Wang, Z.Y., Liu, G.C., Zheng, H., Li, F.M., Ngo, H.H., Guo, W.S., Liu, C., Chen, L., Xing, B. S., 2015. Investigating the mechanisms of biochar's removal of lead from solution. Bioresour. Technol 177, 308–317. https://doi.org/10.1016/j.biortech.2014.11.077.
Worku, Z., Tibebu, S., Nure, J.F., Tibebu, S., Moyo, W., Ambaye, A.D., Nkambule, T.T.I., 2023. Adsorption of chromium from electroplating wastewater using activated carbon developed from water hyacinth. Bmc Chem. 17 (1). https://doi.org/10.1186/s13065-023-00993-4.
Xiao, H.Y., Lin, Q.M., Li, G.T., Zhao, X.R., Li, J.Z., Li, E.Z., 2022. Comparison of biochar properties from 5 kinds of halophyte produced by slow pyrolysis at 500 °C. Biochar. 4 (1). https://doi.org/10.1007/s42773-022-00141-6.
Xie, X., Cao, M., Tu, S., Xiong, S., Zheng, M., 2025. Adsorption performance of Cd(II) and As(III) in aqueous solution by iron-manganese modified biochar synthesized via microwave-assisted low-temperature oxidation. J. Environ. Chem. Eng. 13 (5), 118073. https://doi.org/10.1016/j.jece.2025.118073.
Xu, R., Wei, J., Cheng, D., Wang, W., Hong, L., Chen, Y., Guo, Y., 2024. Abundant porous biochar derived from luffa vine for removal of methylene blue: selective adsorption and mechanistic studies. Ind. Crops. Prod. 219, 119114. https://doi.org/10.1016/j.indcrop.2024.119114.
Yan, X., Dong, X.C., Zhang, W., Yin, H.X., Xiao, H.L., Chen, P., Ma, X.F., 2014. Reference gene selection for quantitative real-time PCR normalization in *Reaumuria soongorica*. PLoS. One 9 (8). https://doi.org/10.1371/journal.pone.0104124.
Yang, J.P., Cheng, S.P., Wang, Y.Q., Li, L.L., Lu, S.Y., 2025. Ecological restoration orientated application and modification of constructed wetland substrates. Env. Res 267. https://doi.org/10.1016/j.envres.2024.120635.
Ye, Z.J., Jiang, M.Y., Yan, F.M., Cao, B.Y., Wang, F., 2024. Chemical aging of biochar-zero-valent iron composites in groundwater: impact on Cd(II) and Cr(VI) co-removal. Env. Res 263. https://doi.org/10.1016/j.envres.2024.120022.
Yu, Q.Y., Zhang, X.H., Gao, T., Gong, X.L., Wu, J.R., Tian, S., Ma, B., Xu, L.J., Joseph, S., Zheng, J.F., Bian, R.J., Li, L.Q., 2024. Converting plastic-contaminated agricultural residues into fit-for-purpose biochar soil amendment: an initial study. Biochar. 6 (1). https://doi.org/10.1007/s42773-024-00382-7.
Yuan, Q., Wang, P., Wang, X., Hu, B., Wang, C., Xing, X., 2023. Nano-chlorapatite modification enhancing cadmium(II) adsorption capacity of crop residue biochars. Sci. Total Environ. 865, 161097. https://doi.org/10.1016/j.scitotenv.2022.161097.
Zhang, G.S., Liu, N., Luo, Y., Zhang, H.B., Su, L., Oh, K., Cheng, H.Y., 2021. Efficient removal of Cu(II), Zn(II), and Cd(II) from aqueous solutions by a mineral-rich biochar derived from a spent mushroom (Agaricus bisporus) substrate. Mater. (Basel) 14 (1). https://doi.org/10.3390/ma14010035.
Zhang, H., Li, R., Zhang, Z., 2022a. A versatile EDTA and chitosan bi-functionalized magnetic bamboo biochar for simultaneous removal of methyl orange and heavy metals from complex wastewater. Env. Pollut 293, 118517. https://doi.org/10.1016/j.envpol.2021.118517.
Zhang, H., Shao, J.G., Zhang, S.H., Zhang, X., Chen, H.P., 2020. Effect of phosphorus-modified biochars on immobilization of Cu (II), Cd (II), and As (V) in paddy soil. J. Hazard. Mater 390, 8. https://doi.org/10.1016/j.jhazmat.2019.121349.
Zhang, J., Li, P., Li, L., Zhao, M., Yan, P., Liu, Y., Li, W., Ding, S., Zhao, Q., 2025a. Soil respiration and carbon sequestration response to short-term fertilization in wheat-maize cropping system in the North China Plain. Soil Tillage Res. 251, 106536. https://doi.org/10.1016/j.still.2025.106536.
Zhang, L., Zhang, Z., Wang, L., Guo, Z., Luo, Y., Tang, K.H.D., Li, M.-L., Li, R.-H., 2025b. Mechanism and application of sulfhydryl-modified chitosan derivative for decontamination of Pb(II) and Cd(II) in water bodies. Int. J. Biol. Macromol 306, 141535. https://doi.org/10.1016/j.ijbiomac.2025.141535.
Zhang, P., Xue, B., Jiao, L., Meng, X., Zhang, L., Li, B., Sun, H., 2022b. Preparation of ball-milled phosphorus-loaded biochar and its highly effective remediation for Cd- and Pb-contaminated alkaline soil. Sci. Total Environ. 813, 152648. https://doi.org/10.1016/j.scitotenv.2021.152648.
Zhang, S.H., Zhang, H., Cai, J., Zhang, X., Zhang, J.J., Shao, J.A., 2018. Evaluation and prediction of CadmiuM removal from aqueous solution by phosphate-modified activated bamboo biochar. Energy Fuels. 32 (4), 4469–4477. https://doi.org/10.1021/acs.energyfuels.7b03159.
Zhu, G., Zhao, Y., Wang, Y., Huang, B., Chen, R., Zhao, X., Wu, P., Tu, Q., 2026. Adsorption characterization and mechanism of a red mud–Lactobacillus plantarum composite biochar for Cd2+ and Pb2+ removal. Biol. (Basel) 15 (2), 153.
Zhu, X.Z., Zhou, Y.P., Yan, Z.H., Yan, Y.F., Li, S.Q., Yu, M.J., Yan, X., Zhang, M.J., 2025. Stabilization effect and mechanism of heavy metals by microbial consortium of phosphate-solubilizing bacteria and urease-producing bacteria. Front. Microbiol. 16. https://doi.org/10.3389/fmicb.2025.1525316.